Structure and hardness of nanocrystalline silver

TOKUSHI KIZUKA *, HIDEKI ICHINOSE ‡, YOICHI ISHIDA‡
Institute of Industrial Science, University of Tokyo, 7-22-1, Roppongi, Minato-ku, Tokyo, 106, Japan

Nanocrystalline silver (Ag) was prepared by *in situ* compacting of ultra-fine silver particles. The structures of as-compacted and annealed specimens were analysed by high-resolution transmission electron microscopy and scanning electron microscopy. Vickers microhardness was measured on the specimens. The ultra-fine particles aggregate before compaction. It is found that the nanocrystalline specimens are obtained by the compaction of the aggregates. Microstructure inside the aggregates does not change as the compacting pressure increases from 0.25 to 2.00 GPa. The compacting pressure affects on the structure and density of the boundaries between the aggregates, i.e. the formation of the crack-type defects of about 1μm at the boundaries. Thermal stability of nanocrystalline Ag is significantly low; grain coarsening starts below 200 °C. However, a nanometre-sized layered structure forms in local regions upon annealing and is stable up to 800 °C. Vickers microhardness of as-compacted specimens increases with increasing compacting pressure. The increase is attributed to the decrease of the number of crack-type defects. Vickers microhardness of nanocrystalline Ag begins to decrease due to grain coarsening upon annealing around 200 °C. The microhardness of nanocrystalline Ag deviates from the Hall–Petch relation.

1. Introduction

Improvement of strengthening in polycrystalline materials by refinement in grain size to micrometre scale has been predicted according to Hall–Petch strengthening theory [1, 2]. However polycrystalline materials of much smaller grain size, nanocrystalline materials, showed novel variation of hardness from micrometre-grained materials. Negative Hall–Petch slopes were reported in nanocrystalline Pd and Cu of average grain size from 6 to 16 nm [3] and nanocrystalline Ni–P of average grain size from 9 to 120 nm [4]. The negative slopes were interpreted as the softening due to the grain-boundary triple-line disclination effect by Palumbo *et al.* [5] or significant increase of grain boundary diffusion by Chokshi *et al.* [3]. On the other hand, it was pointed out by Fougere *et al.* [6] that such novel variation of hardness observed in nanocrystalline materials was dependent on specimen preparation. The negative Hall–Petch slopes were observed in the hardness measurements for a single specimen which was successively annealed to increase grain size [3, 4]. Positive slopes were also reported in nanocrystalline Cu of average grain size from 5 to 50 nm [7, 8] and nanocrystalline Ni of average grain size from 10 to 1000 nm [9] when the hardness was measured on a series of as-prepared specimens. So far these experiments have focused on the relationship between the hardness and grain size. Detailed structural analyses are required to elucidate the variation of hardness in nanocrystalline materials.

In the present study, specimens of bulk nanocrystalline silver (Ag) were prepared by *in situ* compacting of ultra-fine silver particles produced by inert gas evaporation under various compacting pressures from 0.25 to 2.00 GPa. Atomic structures of as-compacted and annealed specimens were observed by high-resolution electron microscopy (HRTEM). Low magnification observation was carried out by scanning electron microscopy (SEM). Vickers microhardness was measured on these specimens.

2. Experimental procedure

Nanocrystalline Ag was prepared by condensation of ultra-fine silver particles without exposure to air as pioneered by Gleiter and co-workers, [10–12] and Kizuka and co-workers [13, 14]. The ultra-fine particles were produced by means of an inert gas evaporation method [15, 16]: silver (99.999%) was evaporated on a tungsten heater in helium at

* Present address: Department of Applied Physics, Faculty of Engineering, Nagoya University, Furo-cho, Chikusa-ku, Nagoya, 464-01, Japan.
‡ Present address: Department of Materials, Faculty of Engineering, University of Tokyo, Hongo, Tokyo, 113, Japan.

0022–2461

1.3×10^2 Pa introduced after evacuation to 10^{-6} Pa in an ultra-high vacuum chamber. The ultra-fine particles moved upwards with the gas flow and adhered to a rotating cylinder kept at liquid nitrogen temperature. After restoring the vacuum chamber to 10^{-6} Pa, the ultra-fine particles were scraped off the cylinder surface and *in situ* compacted into a disc of 5 mm in diameter and 0.5 mm in thickness. The ultra-fine particles were not exposed to air before compaction. The compacting pressure was varied from 0.25 to 2.00 GPa. Coarse grained silvers, with grain size 100 μm, of same external shape were prepared and deformed by 200% for reference. Isochronal annealing was carried out for all specimens from 200 to 800 °C for 1.8×10^3 s in a vacuum of 10^{-2} Pa.

The surfaces of the disc-shaped specimens were observed using a 20 kV scanning electron microscope (JEOL JSM-T20). The disc-shaped specimens for HRTEM were cut into edge-shaped specimens using razor blades. The specimens were observed with a 200 kV high-resolution electron microscope (JEOL JEM-200CX) equipped with a top entry goniometer stage.

The disc-shaped specimens were indented by a diamond pyramid using a Vickers microhardness test machine (Akashi, MVK-HO) over a peak load range of 1 N with a dwell time of 20 s.

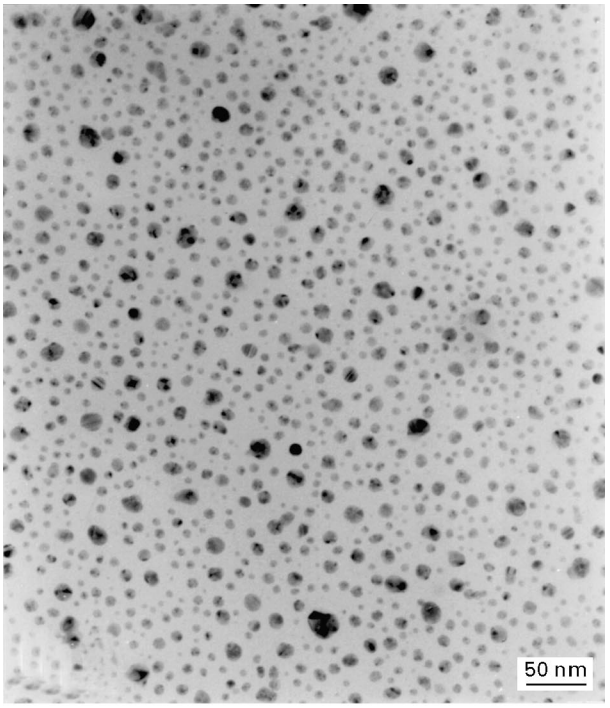

Figure 1 Bright field image of the ultra-fine silver particles before compaction.

3. Results and discussion

3.1. Structure

Fig. 1 shows a bright field image of the ultra-fine particles collected on a micro-grid placed on the surface of a cold cylinder at liquid nitrogen temperature before compaction. The particles are single-crystalline and multiple-twinned particles which are the aggregates of some crystallites containing $(1\,1\,1)/(1\,1\,1)\Sigma = 3$ twin grain boundaries. The size of the particles ranged from 1 to 15 nm.

Fig. 2 shows optical micrographs of surfaces of as-compacted specimens with compacting pressure from 0.25 to 2.00 GPa. SEM micrographs at higher magnification of typical surfaces of the specimens compacted at 0.50 and 2.00 GPa are shown in Fig. 3. Crack-type defects about 1 μm in size, which are unfilled regions at the compaction, are observed on the surface of the specimens with low compacting pressures up to 1.50 GPa. The number of defects decreases and the size becomes smaller as compacting pressure increases. No defect was observed in the specimen compacted at higher pressure, i.e. more than 2.00 GPa. The defect-free region of the surfaces with the low compacting pressure, 0.50 GPa, is similar to that obtained with the high compacting pressure, 2.00 GPa as shown in Fig. 3.

All electron diffraction patterns from selected areas of 1 μm in diameter of as-compacted and annealed specimens consisted of rings corresponding to those of the face centred cubic structure with lattice constant of bulk silver, 0.409 nm; a reaction phase, an amorphous

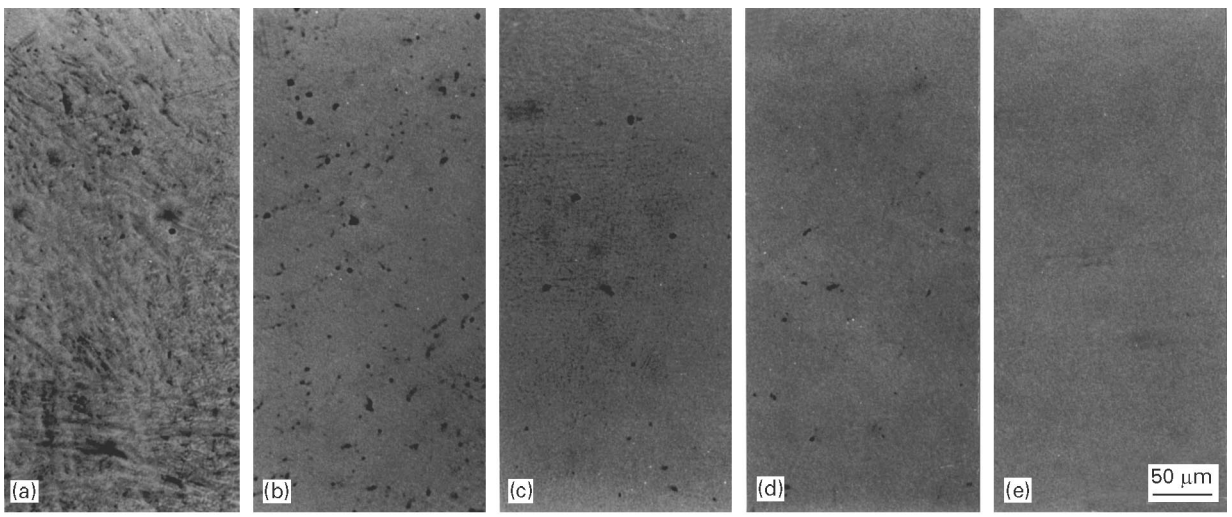

Figure 2 Optical micrographs of surfaces of as-compacted specimens with compacting pressures of (a) 0.25 GPa, (b) 0.50 GPa, (c) 1.00 GPa, (d) 1.50 GPa and (e) 2.00 GPa.

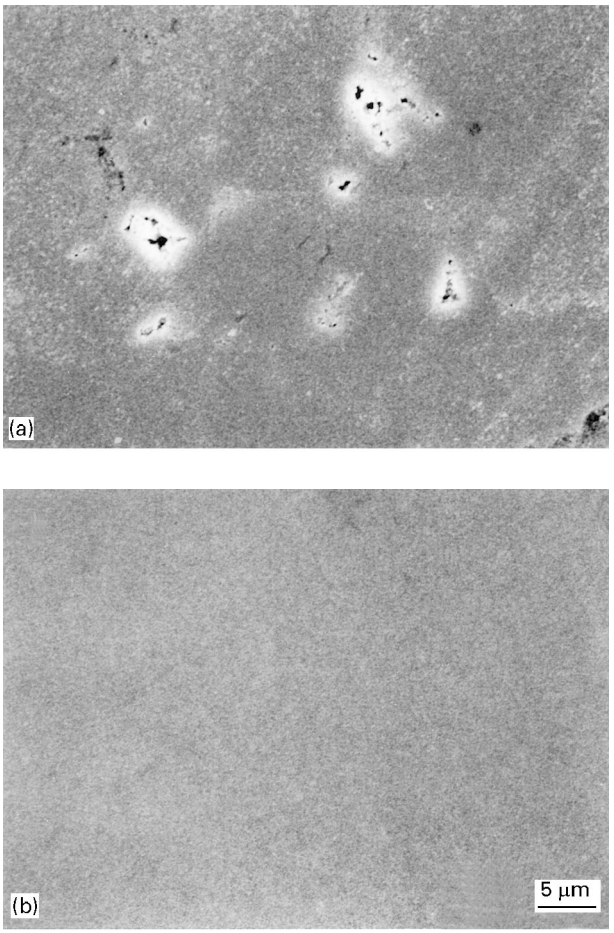

Figure 3 Scanning electron microscope images of surfaces of the specimens compacted at (a) 0.50 GPa and (b) 2.00 GPa.

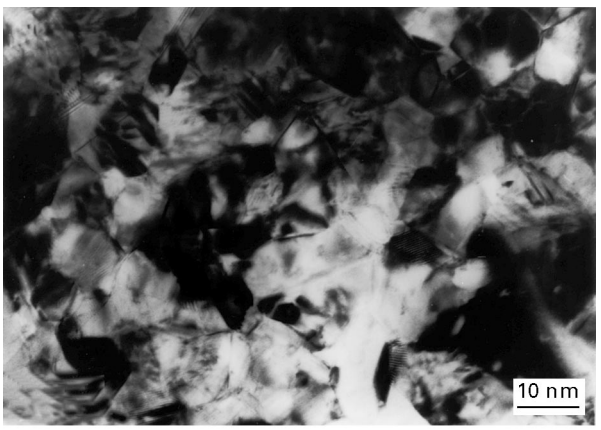

Figure 4 Bright field image of an as-compacted specimen with compacting pressure of 2.00 GPa.

phase or an oxide phase was not identified, and no preferred orientation relationship between grains existed over a large area. X-ray diffraction also showed similar results in the present specimens.

Figs 4 and 5 show a bright field image and a high-resolution image of as-compacted specimen with compacting pressure of 2.00 GPa respectively. The grain size was estimated to be 5–20 nm. The grain size becomes larger than that of the fine particles before compaction, 1–15 nm, indicating that the grains of 1–4 nm in size coarsen on compaction. Positron annihilation

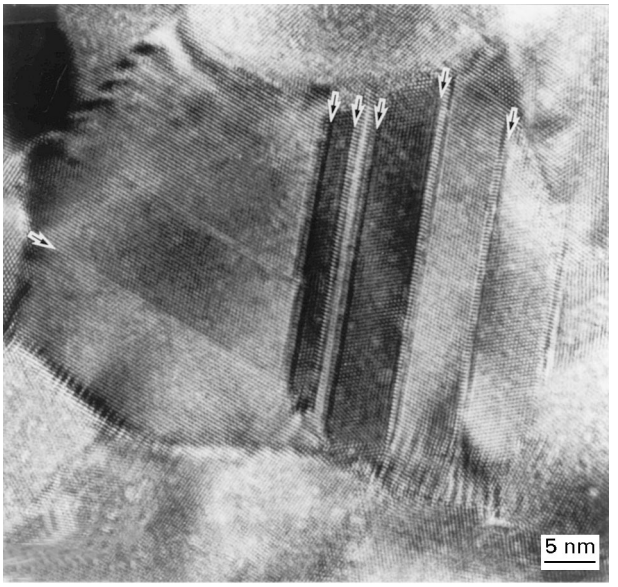

Figure 5 High-resolution image of an as-compacted specimen with compacting pressure of 2.00 GPa.The (1 1 1)/ (1 1 1) $\Sigma = 3$ twin grain boundaries are indicated by arrows.

measurements showed that grain coarsening in nanocrystalline Ag started at 100 °C [13]. Thus nanocrystalline Ag is unstable around room temperature.

The grain boundary length between two adjacent triple points ranges from 2 to 20 nm. Twin grain boundaries, (1 1 1)/(1 1 1) $\Sigma = 3$, were frequently observed in as-compacted specimens as shown by the arrows in Fig. 5. A similar result was reported for nanocrystalline Pd [17]. The twin grain boundary was also dominant in the present ultra-fine silver particles as described above. Stability of grain boundary structure varies as the boundary length decreases [10–12]. The present results show that the twin grain boundary is the most stable when the boundary length ranges from 2 to 20 nm in silver.

Voids of 1–5 nm in diameter, which reduced relative density of the specimens, were observed not inside the grains but on the grain boundaries, particularly on the grain boundary triple points as reported previously [13].

No difference was observed in microstructure, i.e. grain shape, grain size distribution and atomic structures of grain boundaries including grain boundary triple points, of as-compacted specimens with various compacting pressures from 0.25 to 2.00 GPa as shown in Figs 4 and 5 and our previous report [13]. Schaefer *et al.* [18] reported that the positron annihilation lifetimes and the intensities of the components in nanocrystalline Fe did not change in the region of compacting pressure from 0.14 to 4.5 GPa, showing that the structure and density of vacancy cluster type defects at grain boundaries were not affected by the compacting pressure. On the other hand, the number of defects of about 1 μm in the present specimens decreases with increasing compacting pressure. It is considered that the ultra-fine particles aggregate before the compaction, and the crack-type defects are formed at the boundaries between the nanocrystalline aggregates when the compacting pressure is low, i.e.

the as-prepared specimens are produced by the compaction of the nanocrystalline aggregates.

Figs 6 and 7 show bright field images of the specimens annealed at 200 and 400 °C, respectively. Two types of grain coarsening are observed during annealing at 200 °C as shown in Fig. 6. In one area, grains coarsen isotropically to a size of 20–50 nm. In another area, a layered structure forms; grains elongate two-dimensionally parallel to (1 1 1) lattice planes up to 100–300 nm and do not grow perpendicular to the (1 1 1) planes. The plate-shaped grains of 1–10 nm in thickness bond to the (1 1 1)/(1 1 1) $\Sigma = 3$ twin boundaries. The layered structure is a one-dimensional nanometre structure. Grain coarsening proceeded further upon annealing as shown in Fig. 7. Grains grew isotropically up to 80–100 nm at 400 °C, 200–800 nm at 600 °C and 500–1000 nm at 800 °C. In the area of the layered structure, the grains hardly grew along the direction perpendicular to (1 1 1) planes upon annealing at 800 °C as shown in Fig. 8. Thus, the layered structure is stable even at 800 °C. The layered structure is responsible for the reduction of the estimation of the average grain size by X ray line broadening measurement as performed in several studies [4, 6, 9, 19–21]. Electron microscopy is required to evaluate the texture of the specimens prepared by annealing of nanocrystalline materials.

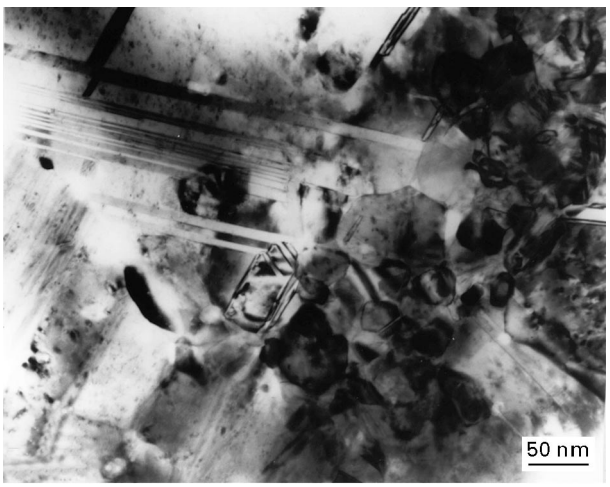

Figure 6 Bright field image of the specimens annealed at 200 °C. The compacting pressure of the specimen is 2.00 GPa.

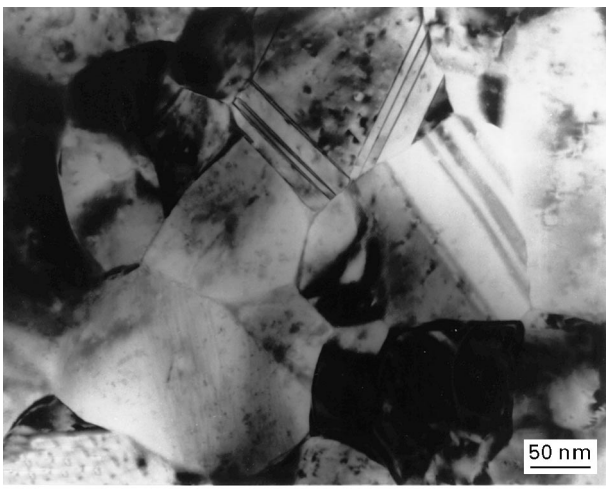

Figure 7 Bright field image of the specimens annealed at 400 °C. The compacting pressure of the specimen is 2.00 GPa.

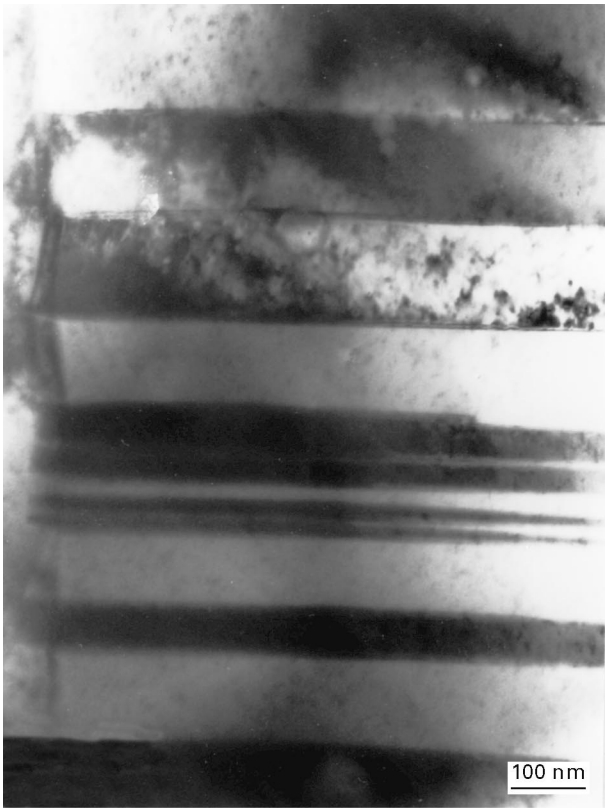

Figure 8 Bright field image of the layered structure in the specimens annealed at 800 °C. The compacting pressure of the specimen is 2.00 GPa.

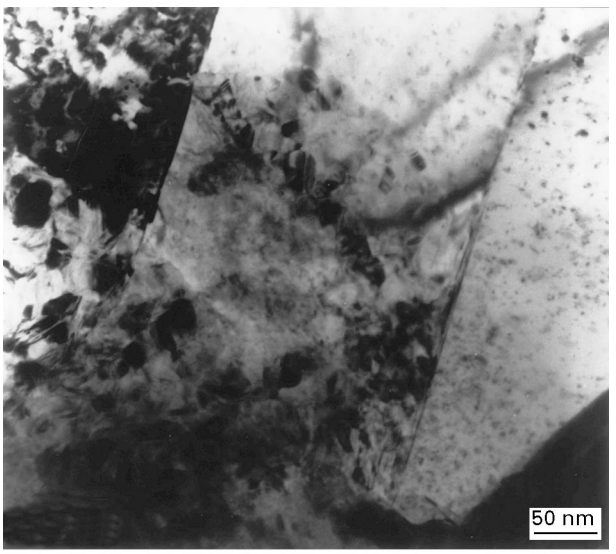

Figure 9 Bright field image of the nanocrystalline structure in the specimen annealed at 600 °C. The compacting pressure of the specimen is 2.00 GPa.

Most of the grains coarsened upon annealing above 200 °C as described above. However a nanocrystalline structure, in which grain size distribution was similar to that of the as-compacted specimens, was observed in the specimens annealed above one half of the melting temperature of bulk silver, 400–800 °C. Fig. 9 shows a bright field image of the nanocrystalline

structure in the specimen annealed at 600 °C. The ratio of the nanocrystalline region was estimated to be 2–3%, 1% and less than 0.1% in the specimens annealed at 400, 600 and 800 °C, respectively.

Gas impurities are introduced in the specimens due to absorption on the surfaces of the ultra-fine particles before compaction [13]. The major component is deduced to be an inert gas, i.e. helium. The other impurities, such as H_2O, H_2 and O_2 remaining as residual gases in the vacuum chamber, are also introduced, but their amount is small compared with that of helium because of the low pressure, 10^{-6} Pa, before introducing helium. A portion of the gases concentrates and forms bubbles at grain boundaries and grain boundary triple points during annealing as shown by positron annihilation measurements [13]. Grain coarsening is depressed by the bubbles because they hinder grain boundary migration [22]. It is deduced that grain coarsening is depressed by the bubbles in the gas-concentrated regions in the present annealed specimens.

3.2. Vickers microhardness

Fig. 10 shows the changes of the Vickers microhardness of as-compacted and annealed specimens as a function of compacting pressure. The microhardness increases with compacting pressure. The microhardness of the specimens compacted at 2.00 GPa is five times larger than that of the well-annealed silver of 100 μm in grain size. The relationship between the hardness and compacting pressure in annealed specimens is similar to that in as-compacted specimens.

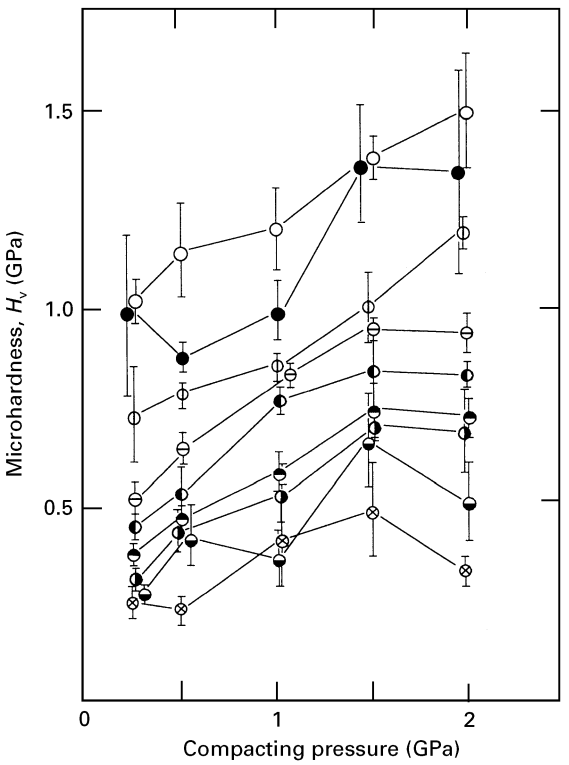

Figure 10 Changes of Vickers microhardness of as-compacted and annealed specimens as a function of compacting pressure. As-compacted specimens are shown by (○) and annealed specimens were shown by (●) 100 °C, (◑) 200 °C, (⊖) 300 °C, (◐) 400 °C, (◓) 500 °C, (◑) 600 °C, (◒) 700 °C and (⊗) 800 °C.

No difference was observed in microstructure by high-resolution observation when compacting pressure changed from 0.25 to 2.00 GPa. On the other hand, the number of crack-type defects of about 1 μm decreased with increasing compacting pressure in the same range. It is inferred that the increase in microhardness with increasing compacting pressure is mainly due to the decrease in the number of crack-type defects rather than the variation in microstructure.

Fig. 11 shows the changes of the microhardness of the specimens prepared under various compacting pressures as a function of annealing temperature. The microhardness of the deformed silver is also shown for reference. The microhardness of all specimens begins to decrease around 200 °C, a third of the melting temperature, and subsequently reduces monotonically to 800 °C. Grain coarsening starts at 200 °C as shown by the present high-resolution observation. The decrease in microhardness with increasing annealing temperature is attributed to grain coarsening.

Nieman *et al.* [7] reported that the microhardness of nanocrystalline Pd was kept up to a half of the melting temperature of bulk Pd, about 500 °C, and decreased rapidly above this temperature. The microhardness of nanocrystalline Au prepared by gas deposition increased upon annealing to 650 °C and decreased above this temperature [23]. Siegel *et al.* [24] investigated the relationship between microhardness and annealing temperature in nanocrystalline TiO_2 (rutile). The microhardness and grain size of nanocrystalline TiO_2 did not change up to about 550 °C. The microhardness rapidly increased due to sintering above 550 °C even though grain coarsening started. Thermal stability of the present nanocrystalline Ag is considerably lower in comparison to nanocrystalline Pd, Au and TiO_2.

The conventional relationship between the hardness (H_v) and grain size (d) for coarse grained materials

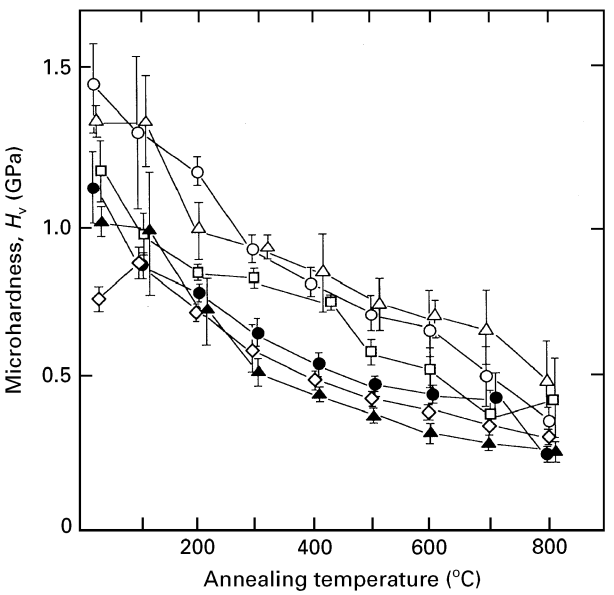

Figure 11 Changes of Vickers microhardness of the specimens prepared under various compacting pressures as a function of annealing temperature. Compacting pressure is shown by (▲) 0.25 GPa, (●) 0.50 GPa, (□) 1.00 GPa, (△) 1.50 GPa and (○) 2.00 GPa. (◇) shows the deformed coarse-grained Ag.

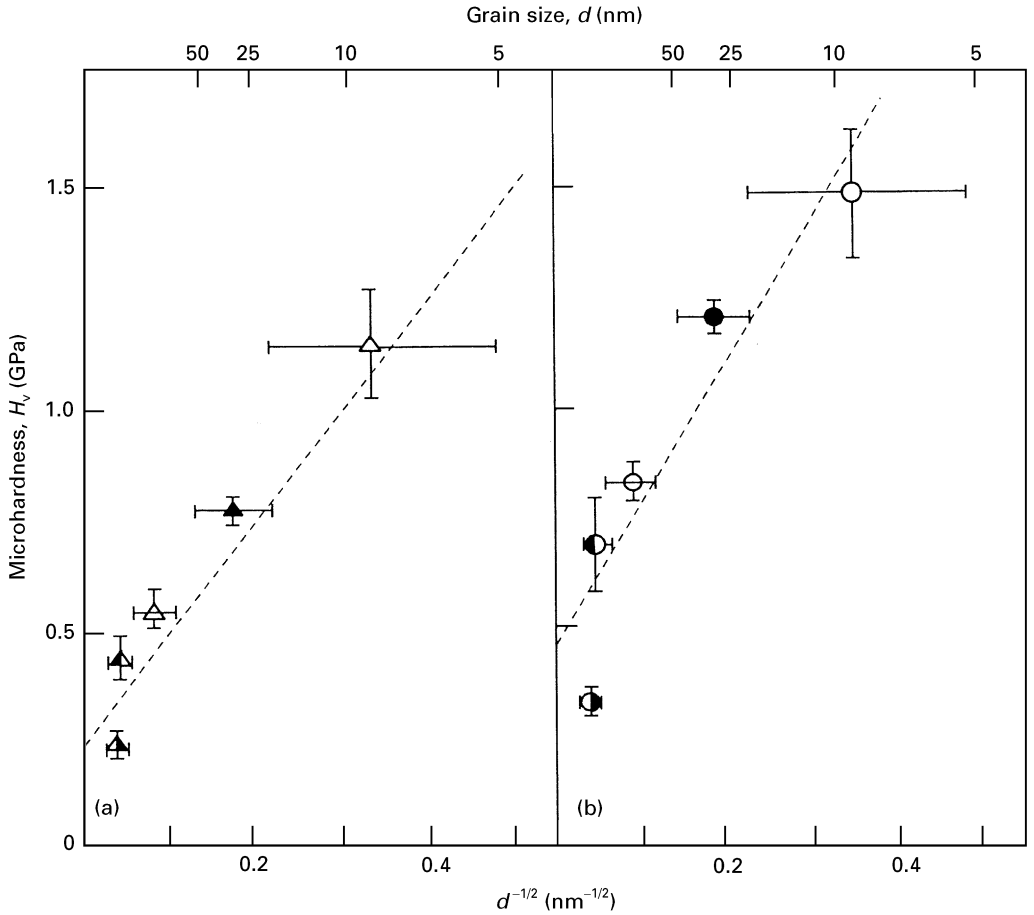

Figure 12 Changes of Vickers microhardness of the specimens compacted at (a) 0.50 GPa and (b) 2.00 GPa as a function of $d^{-1/2}$, where d is the grain size. The hardness of as-compacted specimens is shown by (○, △). The hardness of annealed specimens is shown by (●, ▲) 200 °C, (⊖, ⧋) 400 °C, (◐, ◭) 600 °C and (◑, ◮) 800 °C.

is described by the Hall–Petch equation [1, 2]:

$$H_v = H_0 + kd^{-1/2}$$

where H_0 and k are constants: k is normally positive.

Fig. 12 shows the changes of microhardness of the specimens compacted at 0.50 and 2.00 GPa as a function of $d^{-1/2}$. d was estimated from high-resolution observation. Straight broken lines having positive slopes are extrapolated with the least squares method in Fig. 12. The straight lines are expressed as

$$H_v(\text{GPa}) = 0.24 \pm 0.08\ (\text{GPa}) + (2.6 \pm 0.4)\ (\text{GPa nm}^{1/2})\ d^{-1/2}\ (\text{nm}^{-1/2})$$

for data for the specimen compacted at 0.50 GPa and

$$H_v(\text{GPa}) = 0.44 \pm 0.15\ (\text{GPa}) + (3.3 \pm 0.7)\ (\text{GPa nm}^{1/2})\ d^{-1/2}\ (\text{nm}^{-1/2})$$

for data for the specimen compacted at 2.00 GPa. The data, however, do not fall on straight lines, indicating that the Hall–Petch relation cannot be applied to the present measurement. Three types of relationship between the hardness and grain size were reported for nanocrystalline materials: (i) normal Hall–Petch relation with positive slopes [7–9], (ii) the relationship which deviates from the normal Hall–Petch equation [25] and (iii) an abnormal Hall–Petch relation with negative slopes [3, 4]. The relationship observed in the present study corresponds to type (ii).

The microhardness of the specimens changes as the number of crack-type defects increases. The number of crack-type defects of the specimen compacted at 2.00 GPa is less than that of the specimen compacted at 0.50 GPa. However, the standard deviation of data from the straight line for the specimen compacted at 2.00 GPa in Fig.12b is larger than that for the specimen compacted at 0.50 GPa in Fig.12a. Therefore, the deviation is not attributed to the crack-type defects. The hardness of nanocrystalline Ag inherently deviates from the Hall–Petch equation.

4. Conclusion

The specimens of the bulk nanocrystalline Ag were prepared by *in situ* compacting of ultra-fine particles. The structures of as-compacted and annealed specimens were analysed by HRTEM and SEM. Vickers microhardness was measured on the specimens. The results were as follows.

1. The ultra-fine particles aggregate before compaction. The nanocrystalline specimens are obtained by the compaction of the aggregates.

2. Microstructure inside the aggregates does not change as the compacting pressure increases from 0.25 to 2.00 GPa. The compacting pressure affects the structure and density of the boundaries between the aggregates, i.e. the formation of crack-type defects of about 1 μm at the boundaries.

3. Thermal stability of nanocrystalline Ag is significantly low; grain coarsening starts below 200 °C. However, the layered structure, one-dimensional nanometre structure, forms in local regions upon annealing and is stable up to 800 °C.

4. Vickers microhardness of as-compacted specimens increases with compacting pressure. The increase is attributed to the decrease of the number of crack-type defects.

5. Vickers microhardness of nanocrystalline Ag begins to decrease due to grain coarsening upon annealing at a third of the melting temperature of bulk Ag.

6. The microhardness of nanocrystalline Ag deviates from the normal Hall–Petch relation.

Acknowledgements

The present authors would like to thank The Kazato Foundation, The Okura Kazuchika Memorial Foundation and Yazaki Memorial Foundation for Science and Technology. The present study is partly supported by a Grant-In-Aid of the Ministry of Education, Science and Culture, Japan.

References

1. O. E. HALL, *Proc. Phys. Soc. London* **B64** (1951) 747.
2. N. J. PETCH, *J. Iron Steel Inst.* **174** (1953) 25.
3. A. H. CHOKSHI, A. ROSEN, J. KARCH and H. GLEITER, *Scripta Metall.* **23** (1989) 1679.
4. K. LU, W. D. WEI and J. T. WANG, *Scripta Metall. Mater.* **24** (1990) 2319.
5. G. PALUMBO, U. ERB and K. T. AUST, *ibid.* **24** (1990) 2347.
6. G. E. FOUGERE, J. R. WEERTMAN, R. W. SIEGEL and S. KIM, *ibid.* **26** (1992) 1879.
7. G. W. NIEMAN, J. R. WEERTMAN and R. W. SIEGEL, *Scripta Metall.* **23** (1989) 2013.
8. G. W. NIEMAN, J. R. WEERTMAN and R. W. SIEGEL, *J. Mater Res.* **6** (1991) 1012.
9. G. D. HUGHES, S. D. SMITH, C. S. PANDE, H. R. JOHNSON and R.W. ARMSTRONG, *Scripta Metall.* **20** (1986) 93.
10. R. BIRRINGER, U. HERR and H. GLEITER, *Trans. JIM.* **27** (1986) 43.
11. H. GLEITER, *Prog. Mater. Sci.* **33** (1989) 223.
12. R. BIRRINGER, *Mater. Sci. Eng.* **A117** (1989) 33.
13. T. KIZUKA, Y. NAKAGAMI, T. OHATA, I. KANAZAWA, H. ICHINOSE, H. MURAKAMI and Y. ISHIDA, *Phil. Mag.* **A69** (1994) 551
14. T. KIZUKA, H. ICHINOSE and Y. ISHIDA, *J. Mater. Sci.* **29** (1994) 3107.
15. K. KIMOTO, Y. KAMIYA, M. NONOYAMA and R. UYEDA, *Jpn. J. Appl. Phys.* **2** (1963) 702.
16. R. UYEDA, *Prog. Mater. Sci.* **35** (1991) 1.
17. W. WUNDERICH, Y. ISHIDA and R. MAUER, *Scripta Metall.* **24** (1990) 201.
18. H. E. SCHAEFER, R. WURSCHUM, R. BIRRINGER and H. GLEITER, *Phys. Rev.* **B38** (1988) 9545.
19. B. Z. DING, H. Y. TONG, H. G. JIANG, J. T. WANG and W. D. WEI, *Scripta Metall. Mater.* **28** (1993) 1107.
20. P. G. SANDERS, J. R. WEERTMAN, J. G. BARKER and R. W. SIEGEL, *ibid.* **29** (1993) 91.
21. G. PALUMBO, D. M. DOYLE, A. M. EL-SHERIKT, U. ERBT and K. T. AUST, *ibid.* **25** (1991) 679.
22. Y. LIU and B. R. PATTERSON, *Acta Metall. Mater.* **41** (1993) 2651.
23. S. OKUDA and F. TANG, *Nanostruct. Mater.* **6** (1995) 585.
24. R. W. SIEGEL, S. RAMASAMY, H. HAHN, LI ZONGQUAN, LU TING and R. GRONSKY, *J. Mater. Res.* **3** (1988) 1367.
25. A. M. EL-SHERIK, U. ERB, G. PALUMBO and K. T. AUST, *Scripta Metall. Mater.* **27** (1992) 1185.

Received 19 January
and accepted 17 September 1996